Synthesis, Magnetic Property and Assembly Studies of Two Cu(II) Complexes Based on o-phenanthroline and Phosphate

Fang Fang Jian (ffj2013@163.com)
Henan University of Science and Technology https://orcid.org/0000-0003-3753-2433
E Liu
Henan University of Science and Technology
Zesen Jin
Henan University of Science and Technology
Fangfang Jian
Henan University of Science and Technology

Research Article

Keywords: Copper complexes, One-pot method, Supramolecular, o-Phenanthroline, Phosphoric acid

Posted Date: December 6th, 2021

DOI: https://doi.org/10.21203/rs.3.rs-1109859/v1

Abstract

Using newly precipitated $Cu(OH)_2$, *o*-phenanthroline and phosphoric acid as raw materials, two complicated Cu(II) compounds were obtained by one-pot method. They are double-nuclear Cu(II) **1**, $\{[Cu_2(phen)_2(H_2PO_4)_3][Cu_2(phen)_2(H_2O)(H_2PO_4)_3]\}\cdot 2H_2PO_4\cdot 5H_2O$, and mononuclear Cu(II) 2, $[Cu(phen)_2(H_2PO_4)]_4\cdot 4H_3PO_4\cdot 2HPO_4\cdot 6H_2O$. The crystal structure analysis showed that the copper phosphate reacted with the neutral ligand *o*-phenanthroline to obtain the compounds with different structures. Phosphoric acid can exist in various forms in copper complexes, such as H_3PO_4, $(H_2PO_4)^{1-}$, $(HPO_4)^{2-}$, and form a rich and colorful supramolecular interaction with water molecules. Hirschfeld surface analysis gives the types and regions of molecular interactions in crystals. It is of scientific significance to understand the reaction between transition metal phosphate and organic neutral ligand. The thermogravimetric and magnetic properties of compounds **1** and **2** were also reported. Magnetic analysis shows that supramolecular interactions and dipole-dipole interactions have great influence on the magnetic properties of two compounds.

CCDC: 20565681 for **1**; 2090334 for **2**.

Introduction

Supramolecular self-assembly opens up a pathway for chemists to obtain polymer-like materials by associating small molecules with unconventional polymers [1]. Supramolecular assembly has been shown to provide powerful support for the construction of molecular spherical structures, sensors, host-guest chemistry, catalysis, drug delivery systems, and biomedical applications [2, 3]. Compared with typical strong bonds such as covalent bonds and coordination bonds, secondary bonds that rely on the combination of hydrogen bonds and van der Waals forces will result in micro/nanostructures with unique morphology and properties [4]. In the field of functional structure manufacturing, operations based on supramolecular self-assembly have attracted more and more attention [5]. By chemical modification of supramolecular structures, a large number of highly ordered supramolecular structures can be obtained through different synthesis methods, changing the composition of solvents, temperature and other external fields [6].

Phosphoric acid is a good building block for small molecules. In phosphoric acid, the P atom is sp^3 hybridized and the three hybridized orbitals form three *σ*-bonds with the oxygen atom. The other P-O bond consists of a P to oxygen *σ*-bond and two *d-pπ* bonds from oxygen to phosphorus. Phosphate is a nutrient for all life forms. Phosphoric acid can form ionic bonds with main group metals, such as sodium phosphate (Na_3PO_4), sodium mono-hydrogen phosphate (Na_2HPO_4), sodium di-hydrogen phosphate (NaH_2PO_4), sodium pyrophosphate ($Na_4P_2O_7$), etc. and can also form coordination bonds with transition metals [7]. Phosphate, mono-hydrogen phosphate and dihydrogen phosphate can convert to each other with the change of PH value in the solution, providing abundant channels for supramolecular self-assembly. In living organisms, phosphoric acid functional groups can combine with various functional

groups in the form of hydrogen bonds, causing various biological effects [8]. Examples of multi-component self-assembly of supra- molecular phosphatases are rare, although some artificial models for the hydrolysis of monophosphate phosphates by natural binuclear metallases, such as alkaline phosphatases, have been reported [9]. Considering that phosphorus is attached to four electronegative oxygen atoms rendering the acidity of the P-OH units has been higher and consequently more reactive. And, the reaction of phosphate metal compounds with neutral ligands can construct complexes with one-dimensional, two-dimensional and three-dimensional networks. The study of the structure and properties of phosphate metal complexes can not only enrich the theoretical and experimental research of synthetic chemistry but also obtain novel complexes with novel structures. Moreover, Hirshfeld surface analysis can reveals the interaction forces between neighboring molecules and atoms, and clearly reveals the bond energy connections within and between molecules according to the electron cloud density. It is also a new visual method for studying supramolecular chemistry. More structural information can be obtained by Hirshfeld surface analysis. In this paper, we have synthesized two new compounds from phosphoric acid, copper hydroxide, and *o*-phenanthroline. Their crystal structures are reported, the supramolecular interactions in their crystal structures are studied by Hirshfeld surface analysis method. Also, the magnetic properties and thermal stability of two complexes are analyzed in this paper.

Results And Discussion

A summary of the key crystallographic information for complexes **1** and **2** was given in Supporting Information (**SI**) Table S1 and Table S5, respectively. The bond lengths and bond angles of complexes **1** and **2** by X-ray diffractions are listed in **SI** Table S2, S3, S6, S7. The structural units of two complexes are made up of host $[Cu_2(phen)_2(H_2PO_4)_3(H_2O)]^{1+}$ and $[Cu_2(phen)_2(H_2PO_4)_3]^{1+}$ units, and guest two $(H_2PO_4)^{1-}$ and five H_2O molecules for **1** (Figure 1), and host four $[Cu(phen)_2(H_2PO_4)]^{+}$ and guest one $[(H_3PO_4)_4(HPO_4)_2]^{4-}$ and six H_2O molecules for **2** (Figure 2**)**, respectively. Cu atom in complexes **1** and **2** have five-coordination configurations. According to the determination of five-coordination environmental configuration in literature reported before [10], the τ value of complex **1** is 0.033, while τ value of complex **2** is 1.500. Thus, the coordination configuration of the central copper atom in complex **1** is best described as a slightly distorted tetragonal pyramid geometry. And, complex **2** is best described as a twisted triangular bipyramidal geometry. The Cu-N bond lengths 1.96(2)Å ~ 2.03(2)Å for **1**, 2.00(2)Å ~ 2.12(3)Å for **2**, and N-Cu-N bond angles 80.4(9)°~83.7(8)° for **1**, 79.4(1)° ~ 96.5(1)° for **2**, are in good agreement with the similar structures we reported before [11].

In complex **1**, the four Cu atoms can be thought of as consisting of two dispersed binuclear copper groups. Cu1 and Cu2 coordinate with an *o*-phenanthroline ligand to form a five-member chelating ring. Then, Cu1 and Cu2 are bridged by two P-O bonds of one $(H_2PO_4)^{1-}$ and two O atoms of the other two $(H_2PO_4)^{1-}$ (Figure S2 in **SI**). Cu3 and Cu4 also form a five-member chelating ring with *o*-phenanthroline, and they are bridged by two O atoms in two $(H_2PO_4)^{1-}$. But the coordination group *o*-phenanthroline opposite ligand is H_2O molecule for Cu3 and is $(H_2PO_4)^{1-}$ a group for Cu4, respectively (Figure S3 in **SI**).

The four Cu atoms all form a tetragonal pyramid geometry and the equatorial position is occupied by bridged O atoms in $(H_2PO_4)^{1-}$. The Cu-O bond length are all within reasonable limits. The longest Cu-O bonds are located at the vertices of the tetragonal pyramid, and the bond lengths are Cu1-O11 2.26(3)Å, Cu2-O6 2.31(1)Å, Cu3-O14 2.32(1)Å and Cu4-O22 2.37Å, respectively. Therefore, the main part of complex **1** is best represented by the molecular formula $\{[Cu_2(phen)_2(H_2PO_4)_3][[Cu_2(phen)_2(H_2O)(H_2PO_4)_3]\}^{2+}$, two $(H_2PO_4)^{1-}$ anion equilibrium charge, five solvate water molecules.

The host of complex **2** consists of four dispersed distort trigonal bipyramid $[Cu(phen)_2\ (H_2PO_4)]^{1+}$ groups. The two planes of phenanthroline are almost perpendicular, with an angle of 80.02ºto 81.39ºbetween them. $[H_2PO_4]^{1-}$ is located at the triangular plane and the Cu-O bond lengths are 1.96(3)Å for Cu1-O1, 1.91(2)Å for Cu2-O8, 1.97(3)Å for Cu3-O12, 1.91(2)Å for Cu4-O13, respectively. Since complex **2** has 10 phosphorus atoms in its formula, and neither phenanthroline ligand nor water molecules is charged, the positively charged Cu^{2+} should be in balance with the negatively charged phosphoric acid. According to crystal resolution, 10 phosphorus atoms should be four electrically neutral H_3PO_4, four $(H_2PO_4)^{1-}$ anion, and two $(HPO_4)^{2-}$ anion. According to the length of P-O bond and the coordination strength of hydroxyl oxygen and carbonyl oxygen, complex **2** should be composed of four $[Cu(phen)_2(H_2PO_4)]^{1+}$, two $(HPO_4)^{2-}$, four neutral H_3PO_4 and six H_2O molecules. Therefore, complex **2** is best represented by $[Cu(phen)_2(H_2PO_4)]_4{\cdot}4H_3PO_4{\cdot}2HPO_4{\cdot}6H_2O$.

Secondary bonds play an important role in the construction of complexes [12]. Two complexes all exhibit a variety of types of secondary interactions between host and guest. For complex **1**, the five H_2O molecules are divided into two groups, one consisting of three water molecules, O*w*35, O*w*37 and O*w*38, forming discrete chain $(H_2O)_3$, and the other consisting of O*w*34 and O*w*36, forming a hole chain with two $(H_2PO_4)^{1-}$ anion (Figure S4 in **SI**). In discrete $(H_2O)_3$ water cluster, the O*w*···O*w* distances are 2.686Å for O*w*35···O*w*37 and 2.828Å for O*w*37···O*w*38, these values all in agreement with those in ice *Ih* [13], which suggest a strong H-bonds action. The O*w*35, O*w*37 and O*w*38 connects $[Cu_2(phen)_2(H_2PO_4)_3(H_2O)]^{1+}$ in Cu3 and Cu4 binuclear copper groups with the donor-acceptor distances of 2.617Å, 2.849Å and 3.275Å, respectively. Three water molecules and $[Cu_2(phen)_2(H_2PO_4)_3(H_2O)]^{1+}$ group forms ringlike hydrogen bond network along the *b* axis as shown in Figure 3. The O*w*34 and O*w*36 with two $(H_2PO_4)^{1-}$ anion connects $[Cu_2(phen)_2\ (H_2PO_4)_3]^{1+}$ in Cu1 and Cu2 with the donor-acceptor distances of O*w*34-O26 2.534Å, O*w*34-O8 2.843Å, O*w*34-O31 2.662Å, O*w*36-O27 2.524Å, O*w*36-O33 2.781Å and O*w*36-O2 2.951Å, respectively. The unit of $2H_2PO_4{\cdot}2H_2O$ forms supramolecular large ring with $(H_2PO_4)^{1-}$ group of P8 being the connection point, and $[Cu_2(phen)_2\ (H_2PO_4)_3]^{1+}$ groups are located on either side of the large supramolecular ring as shown in Figure 4.

In addition, the two sets of supramolecular assembly units, $[Cu_2(phen)_2(H_2PO_4)_3(H_2O)]3H_2O$ and $[Cu_2(phen)_2(H_2PO_4)_3]{\cdot}2H_2PO_4{\cdot}2H_2O$, are related, although there is no crossover or association between the two supramolecular large rings, $[(H_2PO_4)_4(H_2O)](H_2O)_3$ and $[(H_2PO_4)_2](H_2O)_2$. Both binuclear copper

host have three $(H_2PO_4)^{1-}$ ligands. These $(H_2PO_4)^{1-}$ ligand bind two sets of supramolecular assembly units, $[(H_2PO_4)_4(H_2O)](H_2O)_3$ and $[(H_2PO_4)_2](H_2O)_2$, together by hydrogen bonding. There are the strong H-bonds actions between $[Cu_2(phen)_2(H_2PO_4)_3(H_2O)]$ $3H_2O$ and $[Cu_2(phen)_2(H_2PO_4)_3]\cdot 2H_2PO_4\cdot 2H_2O$, the donor-acceptor distances of 2.497Å and 2.551Å for O···O, respectively. Thus, the hydrogen bonding forces of complex **1** are formed into a three-dimensional network. This supramolecular force must have a certain effect on the physical and chemical properties of complex **1**. For example, the thermal stability of complex **1** is good, and its magnetic changes are different from those of binuclear Cu (II) previously reported [14]. Multiple H-bonds interactions make Cu(1) and Cu(2) binuclear groups, Cu(3) and Cu(4) binuclear groups, water cluster $(H_2O)_3$ and hole chain $[(H_2PO_4)(H_2O)]_n$ form an intricate 3D network structure, which makes the crystal structure very stable (See Figure 5).

For complex **2**, there are six H_2O molecules, four neutral H_3PO_4 and two $(HPO_4)^{2-}$ anion in the guest. They form very complex three-dimensional structures by hydrogen bonding, with water molecules acting as donors as bridges connecting receptors (H_3PO_4) and $(HPO_4)^{2-}$ to form large rings. First, O*w*41, O*w*42 and O*w*45 bridge two (H_3PO_4) and two $(HPO_4)^{2-}$ to form a small ring (Fig. 6a). Second, O*w*41~O*w*44 five water molecules bridge seven (H_3PO_4) and three $(HPO_4)^{2-}$ to form a large ring with a diameter of about 14.346Å (Fig. 6b). Then, three H_2O O*w*42, O*w*43 and O*w*44, with six (H_3PO_4) and two $(HPO_4)^{2-}$ form a large ring with a diameter of about 14.371Å. O*w*43, O*w*44 and O*w*45 with eight (H_3PO_4) and two $(HPO_4)^{2-}$ form a large ring with a diameter of about 14.660Å. O*w*41 and O*w*44 with six (H_3PO_4) and four $(HPO_4)^{2-}$ form a large ring with a diameter of about 14.679Å (see Fig. 6c). These large rings interleave each other to form a cage structure with holes about 14Å in diameter (Fig. 7a). The O*w*···O distances are 2.584Å to 3.173Å, which indicates that these hydrogen bond interactions are within the normal range. H_3PO_4, $(H_2PO_4)^{1-}$ and $(HPO_4)^{2-}$ all have OH groups in their structures, which can act as both acceptors and donors to form strong hydrogen bonds. The O···O distances of 2.296Å to 2.734 Å are very strong hydrogen bonds interaction among H_3PO_4, $(H_2PO_4)^{1-}$ and $(HPO_4)^{2-}$ groups. It can be seen that $(H_2PO_4)^{1-}$ is not only a ligand to form a coordinate bond with Cu atoms, but also participates in supramolecular assembly. The host, four $[Cu(phen)_2(H_2PO_4)]^+$ ion, is located in the cage structure formed by supramolecular action and is enclosed in the pores by supramolecular chemical bonds (Fig. 7b). It should be noted that the water molecule *w*H_2O(45) does not participate in the supramolecular assembly of the host and guest, and it is more than 3.5 Å away from other O atoms, indicating that it does not form hydrogen bond interactions with other O atoms, and is only crystal water located in the crystal structure. However, from the thermogravimetric analysis of complex **2**, we found that the water of crystallization *w*H_2O(45) was not significantly different from the other five water molecules, which were all lost at 108.1ºC. This shows that it may be deviation to judge the strength of hydrogen bond force only by the distance of donor-acceptor. This prompted us to further study the supramolecular forces of complexs **1** and **2** by means of Hirschfeld surface analysis. The combination of single-crystal X-ray with Crystal Explorer software enables us to analyze the internal structure and electron cloud configuration of molecules more clearly.

The Hirshfeld surface (HS) is a technique currently used to analyze and verify the types of intermolecular interactions in a crystal lattice. The Hirshfeld surface analysis and finger pattern generated using the Crystal-Explorer software can be used to identify the types and regions of molecular interactions. Hirshfeld surface gives a detailed explanation of the immediate environment of a molecule in a crystal 15]. The 3D Hirshfeld surfaces have been mapped over d_{norm}, shape index, and curvedness for complex **1** and **2** as shown in Figure 8 and 9, respectively. The surfaces are shown as transparent to allow visualization of the molecular moiety around which they were calculated. The d_{norm} surface shows regions with red, blue, and white colors, which indicate contacts with smaller, larger, and closer distances to the sum of van der Waals radii, respectively. Red spots are observed in the d_{norm} surfaces, indicating the presence of close-contacts in the crystal structure, such as classical hydrogen bonds O–H•••O, O-H···N and non-classical interactions, such as C–H•••O and C–H•••H. The shape index surface indicates the presence of π•••π stacking interactions in the crystal structure of this compound, observed by the detached red and blue region [15b]. The curvedness is the measurement of "how much shape" the flat areas of the surface correspond to low values of curvedness, while sharp curvature areas correspond to high values of curvedness, indicating interactions between neighboring molecules. The large flat region indicated by a blue outline on the curvedness surface refers to the π···π stacking interactions of the molecule. The π···π stacking information conveyed by the shape index and curvedness plots are consistent with the crystal structure analyses. As can be seen from Fig. 8 and 9, both complexes **1** and **2** indicate strong hydrogen bonding in solid surface (red pots in d_{norm} and shape index), and significant π···π interactions between phenanthroline ring (blue outline in curvedness). This is consistent with crystal structure analysis.

Hirshfeld 2D fingerprint plots allow quick and easy identification of the significant intermolecular interactions map on the molecular surface [16]. Fingerprint plots of complexes **1** and **2** are represented in Fig. 10 and 11, respectively, and display the intermolecular contacts present in the crystalline solid. From Fig. 10, we can see the main contributions of various supramolecular forces to the crystal structures of the complex **1**. The O•••H and H•••H interactions have the most contribution, with the O•••H interaction contributed of 49.4%, the H•••H interaction contributed 31.0%. The others interaction contributed are C···H 7.4%, π•••π 6.0%, C···N 2.9%, N•••H 1.0%, O···O 0.6%, C···O 0.5%, Cu···H 0.8% and Cu···C 0.4%, which are found in Figure S7 (Left). The main contributions of the supramolecular forces in complex **2** were also the O•••H and H•••H interactions, with O•••H 39.5% and H•••H 34.1%. The others interaction contributed are C···H 10.5%, π•••π 7.8%, C···N 2.1%, N•••H 2.1%, O···O 2.0%, C···O 1.9%, Cu···H 0.1% and Cu···C 0%, which are found in Figure S7 (Right).

To get more insight into the properties relative to supramolecular interaction for complexes **1** and **2**, their dehydration behavior has been investigated using thermogravimetric analysis. Complex **1** and **2** all have water clusters in their structure. To the best of our knowledge, the losses of all water molecules in neutral water clusters are all below 140°C [17]. The losses of the coordinated water molecules in crystal we found so far the highest dehydration temperature was 225°C [18]. H_2O molecules in anion water clusters are much stable, which can be existed at higher temperature. The TGA and DTG curves of complex **1**,

{[$Cu_2(phen)_2(H_2PO_4)_3$][$Cu_2(phen)_2(H_2O)$ ($H_2PO_4)_3$]}·$2H_2PO_4$·$5H_2O$, are illustrated in Fig. 12a. These supramolecular interactions keep the light at higher thermal stability, it loses water molecules when they were heating to 117.9ºC under N_2 atmospheric pressure. Complex **1** has four obvious weightlessness processes accompanied by sharp heat absorption peaks. In the first stage, there was an obvious heat absorption peak at 117.9ºC, and the loss of 4.75% indicated that five water molecules were lost. Combined with crystal structure analysis, it is speculated that five water molecules in the structure are lost completely. In the second stage, the weight loss was at 247.4ºC with an obvious heat absorption peak. The weight loss of 5.00% was presumed to be the removal of H_3PO_4 molecules (calc. 5.17%). In the third stage, the weight loss was 4.09%, and the heat absorption peak was 367.0ºC, indicating that two H_3PO_4 began to decompose or react, and the residual chemical formula was $Cu_4(phen)_4(PO_4)(H_2PO_4)_5$ (found 86.17% calc. 86.18%). In the fourth stage, it loses 11.2% weight with the absorption peak at 509.9ºC, indicating that the residue may be $Cu_4(phen)_4$ $(PO_4)_2(H_2PO_4)_2$ (found 74.97% calc. 75.80%).

The TGA and DTG curves of the complex **2**, $[Cu(phen)_2(H_2PO_4)]_4$·$4H_3PO_4$·$2HPO_4$·$6H_2O$, are illustrated in Fig. 12b. There are five stages of decomposition for complex **2**. In the first stage, it loses 3.96% with an obvious heat absorption peak at 108.1ºC, which indicated that six water molecules were lost completely (calc. 3.89%). In the second stage, the weight loss was 7.01% with a heat absorption peak at 251.0ºC, which suggests the removal of two H_3PO_4 molecules (calc. 7.06%). In the third stage, the weight loss was 15.11%, and the heat absorption peak at 370.8ºC, indicating that H_3PO_4, $(H_2PO_4)^{1-}$ and $(HPO_4)^{2-}$ group maybe began to decompose. In the fourth stage, it loses 6.21% weight with the absorption peak at 426.1ºC, and the residual chemical formula was $Cu_4(phen)_8(P_2O_7)(O)_2$ (found 73.92% calc. 74.21%). The fifth stage, the absorption peak at 481.0ºC, weight loss of 6.56%, suggests that the residue may be $[Cu_4(phen)_8](O)_4$ (found 61.16% calc. 69.10%). The large error of this formula indicates that the *o*-phenanthroline ligands may also decompose or lose at this temperature. At 898.9°C, the final residual weight was still 44.44%, indicating that *o*-phenanthroline had not been completely lost, and the final residual molecular formula was probably $Cu_4(phen)_4(P_2O_7)(O)_2$ (calc. 45.39%).

The variable-temperature magnetic properties of complex **1** are shown in Figure 13 (Left) in the form of $\chi_M T$ versus T. At room temperature, the product of $\chi_M T$ is 0.85 emu·K·mol^{-1}, corresponding to the theoretical value of two spin-only Cu(II) ions with S = 1/2 and g > 2 due to the spin-orbital contribution. Upon cooling, $\chi_M T$ increases very slowly and almost keep a constant from 300 to 10 K, and then quickly increase a little to 0.89 emu·K·mol^{-1} at 2 K, indicating the very weak ferromagnetic coupling between Cu(II) ions in the dinuclear complex. The magnetic properties can be fitted using Heisenberg-Dirac-van Vleck S_1 = S_2 = 1/2 spin-coupled dimer model ($\mathbf{H} = -2J\mathbf{S_1}\cdot\mathbf{S_2}$), where J is the coupling constant between two Cu(II) ions. The best fitting results gave: g = 2.123(2) and J = 0.15(2) cm^{-1} with $R = \sum[(\chi_M T)_{calc} - (\chi_M T)_{obs}]^2/\sum(\chi_M T)^2_{obs} = 8.2 \times 10^{-5}$ as shown in Figure 13 (Left: solid line). The small positive J value indicates very weak ferromagnetic coupling between Cu(II) ions mediated by μ_2-phosphate in complex **1**. Factually, the weak ferromagnetic coupling between spins is easy to be understood. In the structure of **1**, both of Cu1 and Cu2 locate in the square pyramidal coordination environment, so they have the same

magnetic orbital of $d_{x^2-y^2}$. Two μ_2-phosphate ions bridge between Cu1 and Cu2 *via* axis direction of Cu1 and equatorial plane of Cu2 or axis direction of Cu2 and equatorial plane of Cu1. In addition, two equatorial planes for two copper ions are almost parallel. Such a structural arrangement leads to their magnetic orbitals to be orthogonal causing ferromagnetic coupling. At the same time, the coupling interaction is mediated through the lengthened axis because of the Jahn-Teller effect. Therefore, the coupling is very weak. In the unit cell of **1**, there are two molecules with [Cu1Cu2] and [Cu3Cu4]. However, their structures are almost the same, so the magnetic properties of two molecules can be considered equivalent.

Complex **2** shows the very different magnetic properties from **1** because their structures are different. Complex **1** can be regarded as a mononuclear species relative to **2**. Thus, complex **2** should shows the paramagnetic behavior. As expected, the variable-temperature magnetic susceptibilities in the form of $\chi_M T$ are almost a constant of 0.57 emu·K·mol^{-1} above 13 K. Below 13 K, $\chi_M T$ quickly decreases to 0.51 emu·K·mol^{-1} at 2 K. Using the mean-field theory as the molecular interaction zJ for fitting the magnetic properties obtained g = 2.45(1) and zJ = −0.078(1) cm^{-1} with $R = \sum[(\chi_M T)_{calc} - (\chi_M T)_{obs}]^2 / \sum(\chi_M T)^2_{obs}$ = 1.4 × 10^{-6}. The little negative value of zJ indicates the very weak molecular antiferromagnetic interaction in complex **2**. It can be ascribed to the dipole-dipole interaction or π-π interaction between mononuclear molecules.

Conclusion

In summary, two supramolecular self-assembly structures containing H_2O, H_3PO_4, $(H_2PO_4)^{1-}$ and $(HPO_4)^{2-}$, four small molecules building blocks were obtained and characterized by a single X-ray. The guest $[(H_2PO_4)_2(H_2O)_5]^{2-}$ in complex **1** form two supramolecular self-assembly: three discrete water molecules $(H_2O)_3$ and $[(H_2PO_4)_2(H_2O)_2]_n^{2n-}$ anion. While the guest $[(H_3PO_4)_4\,(HPO_4)_2(H_2O)_6]^{4-}$ in complex **2** form a caged structure consisting of several large rings. $(H_2PO_4)^{1-}$ and coordination of water in the host for complex **1**, and $(H_2PO_4)^{1-}$ in the host for complex **2**, are all forming strong supramolecular interactions with the guest. The precise structural information for two complexes helps improve the model of some unexplained properties of small molecules H_2O, H_3PO_4, $(H_2PO_4)^{1-}$ and $(HPO_4)^{2-}$ and understanding better the structure and behavior of those small molecules in the chemical or physical process. These studies show that the hydrogen bond interactions between anions and water molecules are different from those between pure water molecules.

Experimental Section

All manipulations were carried out in air. All solvents, copper sulfate and sodium hydroxide were purchased from National Chemical Reagents Company (Shanghai, China) and used as supplied.

Synthesis of the Complexes 1 and 2

Complexes **1** and **2** are synthesized by the one-pot method. The copper sulfate was dissolved in water and added a considerable amount of sodium hydroxide water solution, then to produce blue precipitation. The precipitation was extracted by pumping and washing with water, fresh copper hydroxide filter cake was obtained. The filter cake was dissolved by 30% phosphoric acid (Note: It is difficult to dissolve 30% H_3PO_4 with aged $Cu(OH)_2$ or copper hydroxide precipitated for too long). After the complete dissolution of copper hydroxide, added *o*-phenanthroline ethanol solution, heated, and refluxing for 3 hours to obtain the purple solution. The purple solution is concentrated and crystallized to produce two crystals of different colors and shapes. The composition of the two complexes was determined by elemental analysis and was justified by single-crystal X-ray diffraction. The formula is $C_{48}H_{60}Cu_4N_8O_{38}P_8$ for **1** and $C_{96}H_{98}Cu_4N_{16}O_{46}P_{10}$ for **2**, respectively. Elemental analysis: for **1:** C%, 30.16 (Calac. 30.97); H%, 3.92 (Calac. 3.28); N%, 5.83 (Calac. 6.02); for **2:** C%, 40.67 (Calac. 41.50); H%, 4.01 (Calac. 3.53); N%, 7.86 (Calac. 8.07).

Physical measurements

Elemental analyses were performed by Perkin-Elmer-240C elemental instrument. Shimadzu TGA-50 Thermogravimetric Analyzer is selected for Thermal analysis. Variable-temperature magnetic susceptibility measurements were performed by Quantum Design PPMS DynaCool magnetometer. The diffraction data were collected on an Enraf-Nonius D/max 2500 diffractometer.

Computational details

CrystalExplorer 17.5 program [19] was used to show the Hirshfeld surfaces and the 2D-fingerprint plots [20]. The crystallographic information files (CIFs) were used as input files. The 3D d_{norm} surfaces (normalized contact distance) were mapped over a fixed color scale of -0.8613 (red) to 2.1439 (blue) for complex **1**, and -0.9907 (red) to 1.5585 (blue) for complex **2**. The d_{norm} property, Eq. (1), is a sum of two distances, d_i and d_e, which are normalized by the Van der Waals radii of the involved atoms. d_i is the closest internal distance from a given point on the surface and d_e is the closest external contact. Equation (1) below:

$$d_{norm} = \frac{d_i - r_i^{vdw}}{r_i^{vdw}} + \frac{d_e - r_i^{vdw}}{r_e^{vdw}}$$

Declarations

Funding

Fangfang Jian received financial support from Special Term Professor financial of Henan University of Science and Technology (13510001), and Luoyang City Talents Plan Fund.

Conflict of interest

The authors declare that there are no conflicts of interest in this work.

Availability of data and material

The authors confirm that the data supporting the findings of this study are available within the article and its supplementary material.

Code availability

Software application

Authors' contributions

E Liu designed, analysis, interpretation of data, and prepared the first draft of the manuscript. Zesen Jin executed the computational work. Fangfang Jian supervised the complete work and critically scrutinized the manuscript.

Ethics approval Not applicable

Consent to participate Not applicable

Consent for publication Not applicable

References

1. Mondal, S.; Ghosh, T. K.; Chowdhury, B.; Ghosh, P. *Inorg. Chem.*, **2019**, *58*, 15993.
2. (a) Inokuma, Y.; Kawano, M.; Fujita, M. *Nat. Chem.*, **2011**, *3*, 349. (b) Zhao, J.; Yang, D.; Yang, X. J.; Wu, B. *Coord. Chem. Rev.*, **2019**, *378*, 415. (c) Li, S.; Huang, J.; Cook, T. R. *J. Am. Chem. Soc.*, **2013**, *135*, 2084. (d) Han, Y. F.; Li, H.; Jin, G. X. *Chem. Commun.*, **2010**, *46*, 6879. (e) Fan, Q. J.; Lin, Y. J.; Hahn, F. E.; Jin, G. X. *Dalton Trans.*, **2018**, *47*, 2240. (f) Gupta, G.; Das, A.; Ghate, N. B. *Chem. Commun.*, **2016**, *52*, 4274.
3. (a) Zhou, J.; Yu, G.; Huang, F. *Chem. Soc. Rev.*, **2017**, *46*, 7021. (b) Gupta, G.; Das, A.; Panja, S. *Chem. Eur. J.*, **2017**, *23*, 17199. (c) Yoon, M.; Srirambalaji, R.; Kim, K. *Chem. Rev.*, **2012**, *112*, 1196. (d) Zhou, J.; Zhang, Y.; Yu, G. *J. Am. Chem. Soc.*, **2016**, *140*, 7730. (e) Cook, T. R.; Vajpayee, V.; Lee, M. H. *Acc. Chem. Res.*, **2013**, *46*, 2464.
4. (a) Sun, Z.; Huang, Q.; He, T. *Chem. Phys. Chem.*, **2014**, *15*, 2421. (b) Jin, H.; Mangun, C. L.; Griffi, A. S. *Adv. Mater.*, **2014**, *26*, 282. (c) Patrick, J. F.; Hart, K. R.; Krull, B. P. *Adv. Mater.*, **2014**, *26*, 4302.
5. (a) Solntsev, P. V.; Anderson, D. R.; Rhoda, H. M. *Cryst. Growth. Des.*, **2016**, *16*, 1027. (b) Zhang, Z.; He, T,; Yuan, M. *Chem. Comm.*, **2015**, *51*, 15862.
6. (a) Cheng, M.; Liu, Q.; Xian, Y.; Shi, F. *ACS Appl. Mater. Interfaces.*, **2014**, *6*, 7572. (b) Zhu, P.; Yan, X.; Su, Y. *Chem. Eur. J.*, **2010**, *16*, 3176. (c) Sun, Z.; Lv, F.; Cao, L. *Angew Chem. Int. Ed.*, **2015**, *54*, 7944. (d) Lu, C.; Guo, W.; Hu, Y. *J. Am. Chem. Soc.*, **2015**, *137*, 15723.

7. Parmar, D.; Sugiono, E.; Raja, S.; Rueping, M. *Chem. Rev.*, **2014**, *114*, 9047.
8. Korhonen, H. J.; Conway, L. P.; Hodgson, D. R. W. *Curr. Opin. Chem. Biol.*, **2014**, *21*, 63.
9. Hisamatsu, Y.; Miyazawa, Y.; Yoneda, K. *Chem. Pharm. Bull.*, **2016**, *64*, 451.
10. Addison, A. W.; Rao, T. N.; Reedijk, J. *J. Chem. Soc. Dalton Trans.,* **1984**, 1349.
11. (a) Jian, F. F.; Lin, J. H.; Zhang, S. S. *Chin. J. Chem.*, **2001**, *19*, 772. (b) Jian, F. F.; Liu, G. Y.; Hao, Q. L. *Chin. Inorg. Chem.*, **2003**, *19*, 419.
12. Casas, J. S.; Castineiras, A.; Rodriguez-Arguelles, M. C. *Coord. Chem. Rev.*, **1999**, *76*, 3.
13. Eisenberg, D.; Kauzmann, W. Oxford University Press: New York **1969**.
14. (a) Kitchen, J. A.; Zhang, N. J.; Carter, A. B. *J. Coord. Chem.*, **2016**, *69*, 2024. (b) Khatua, S.; Kim, K. B.; Kang, J. *Eur. J Inorg. Chem.*, **2009**, *22*, 3266. (c) Jana, S.; Ray, A.' Chandra, A. *ACS Omega*, **2020**, *5*, 274.
15. (a) Dhamodharan, P.; Sathya, K.; Dhandapani, M. *Physica B*. **2017**, *508*, 33. (b) Li, Y.; Zhang, C. G.; Cai, L Y. *J. Coord. Chem*. **2013**, *66*, 3100.
16. (a) Luo, Y. H.; Liu, Q. L.; Yang, L. J. *Res. Chem. Intermed*. **2015**, *41*, 7059. (b) Zhang, J. L.; Zhang, C. L.; Xiao, Y. *Supramol. Chem.***2016**, *28*, 231.
17. (a) Li, Z. G.; Wang, G. H.; Niu, J. J. *Acta Crystallogr. C*, *Cryst. Stru. Comm.*, **2007**, *7*, 15. (b) Su,R.; Li, Y. Z.; Bai, J. F.; Pan, Y. *Cryst. Growth. Des.*, **2007**, *63*, 94. (c) Bernal, I.; Mukhopadhyay, U. *J. Economic Integration*, **2006**, *6*, 363. (d) Beobide, G.; Castillo, O.; Luque, A. *Inorg. Chem.*, **2006**, *45*, 5367. (e) Song, H. H.; Ma, B. Q. *CrystEngComm*, **2007**, *9*, 625.
18. Hong, X. L.; Li, Y. Z.; Hu, H. M. Cryst. Growth. Des., **2006**, *6*, 1221.
19. Wolff, S. K.; Grimwood, D. J.; McKinnon, J. J. *CrystalExplorer 3.1*, University of Western Australia, Australia, **2012**.
20. (a) Nikpour, M.; Mirzaei, M.; Chen, Y. G. Inorg. Chem. Commun. **2009**, *12*, 879. (b) Machini, W. B. S.; David-Parra, D. N.; Teixeira, M. F. S. *Mater. Sci. Eng*. **2015**, *C57*, 344.

Figures

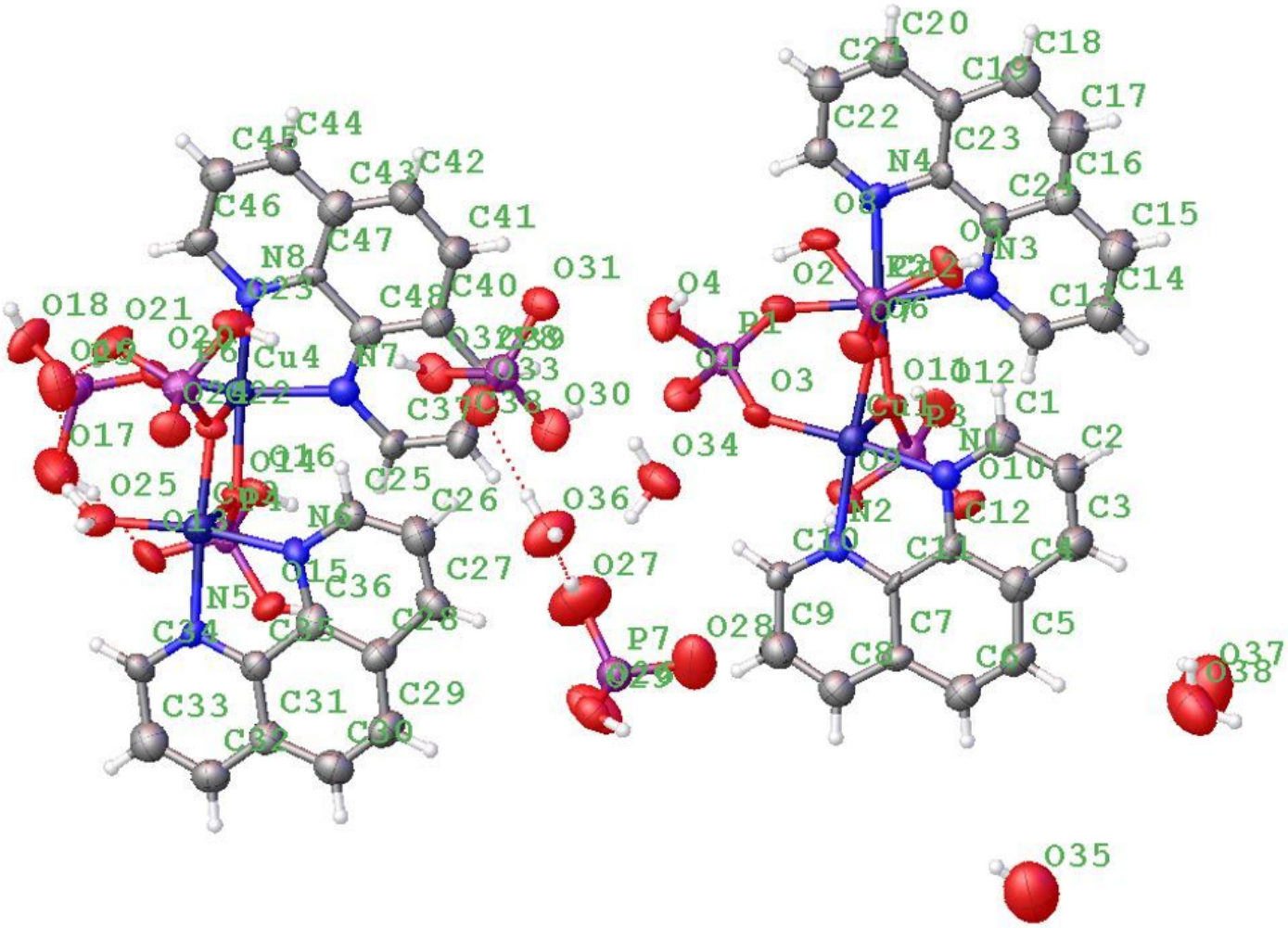

Figure 1

Molecular structure with the atomic numbering scheme for complex 1.

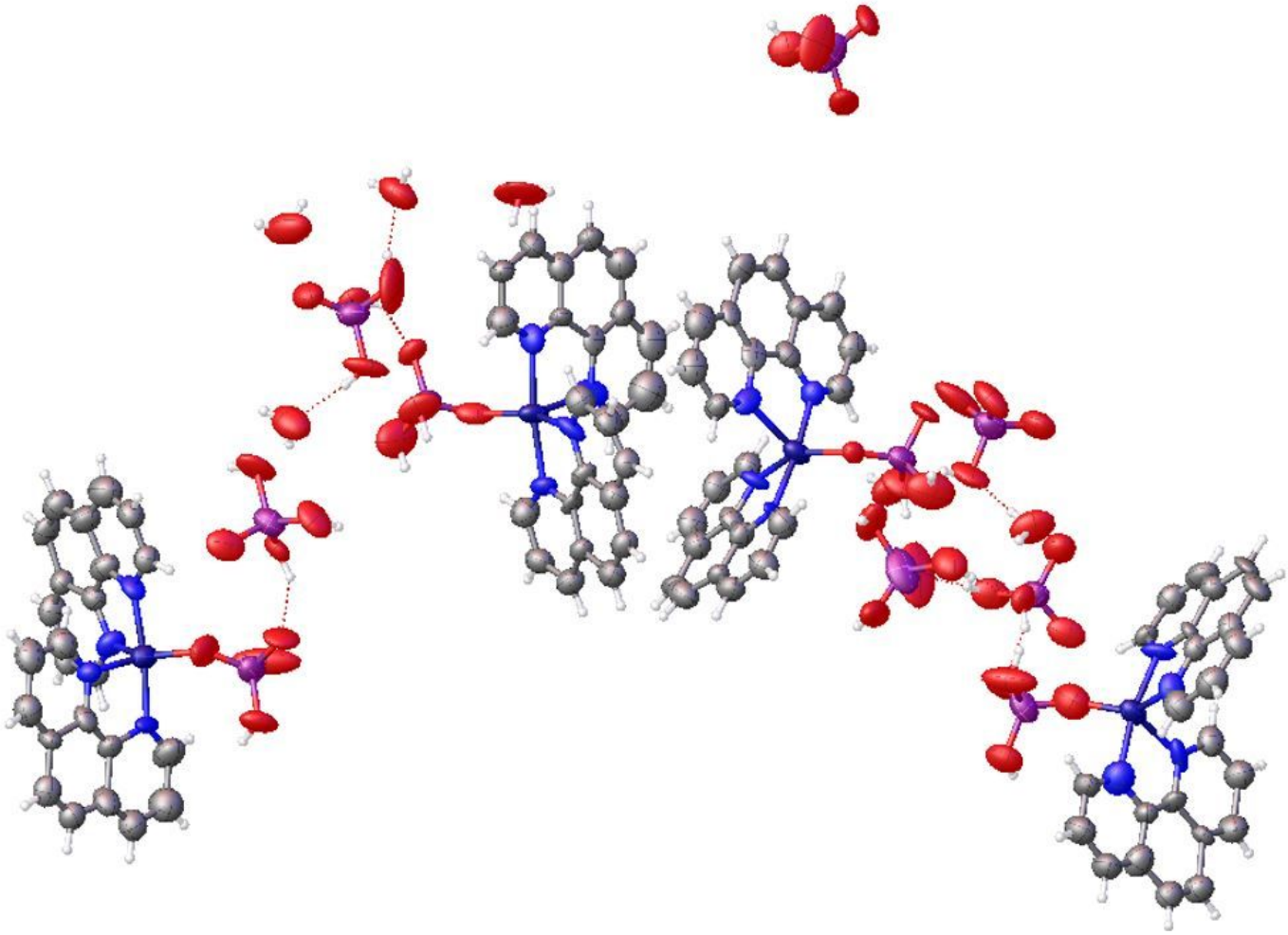

Figure 2

Molecular structure diagram for complex 2.

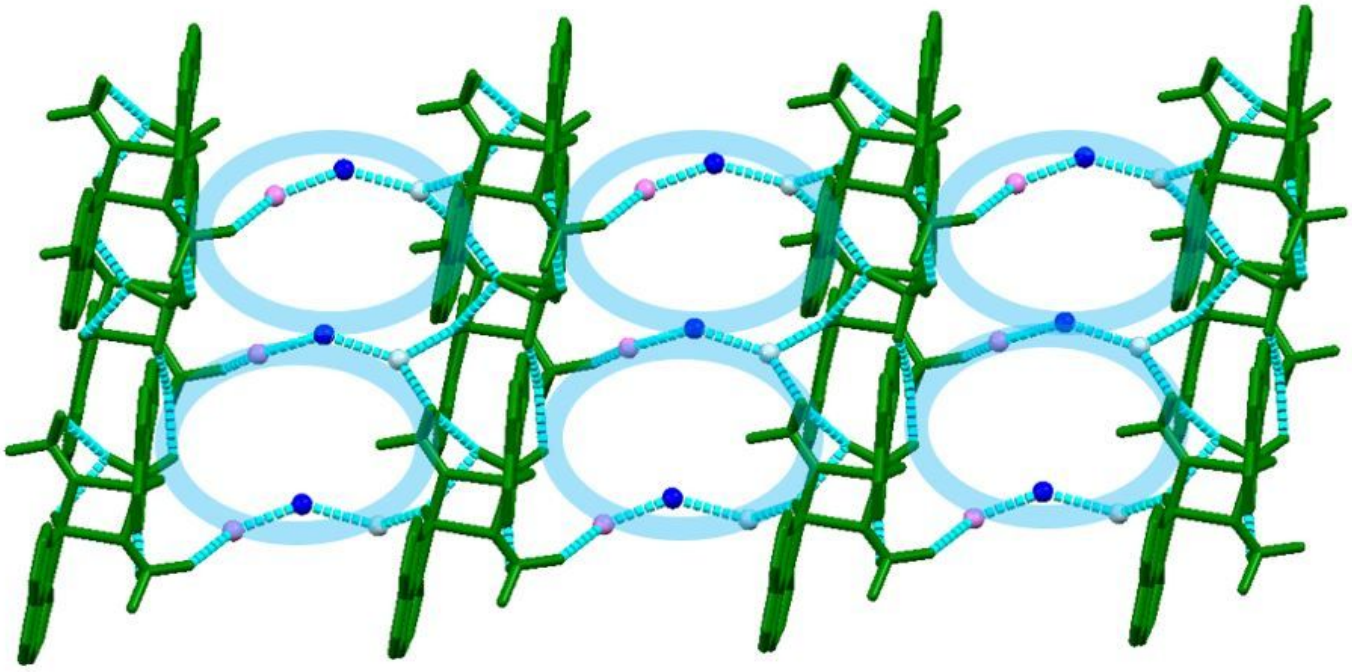

Figure 3

The H-bonds interaction between three water molecules, Ow35 (violet), Ow37 (blue), Ow38 (light blue), with [Cu2(phen)2(H2PO4)3 (H2O)]1+ ion in Cu3, Cu4 binuclear group (green).

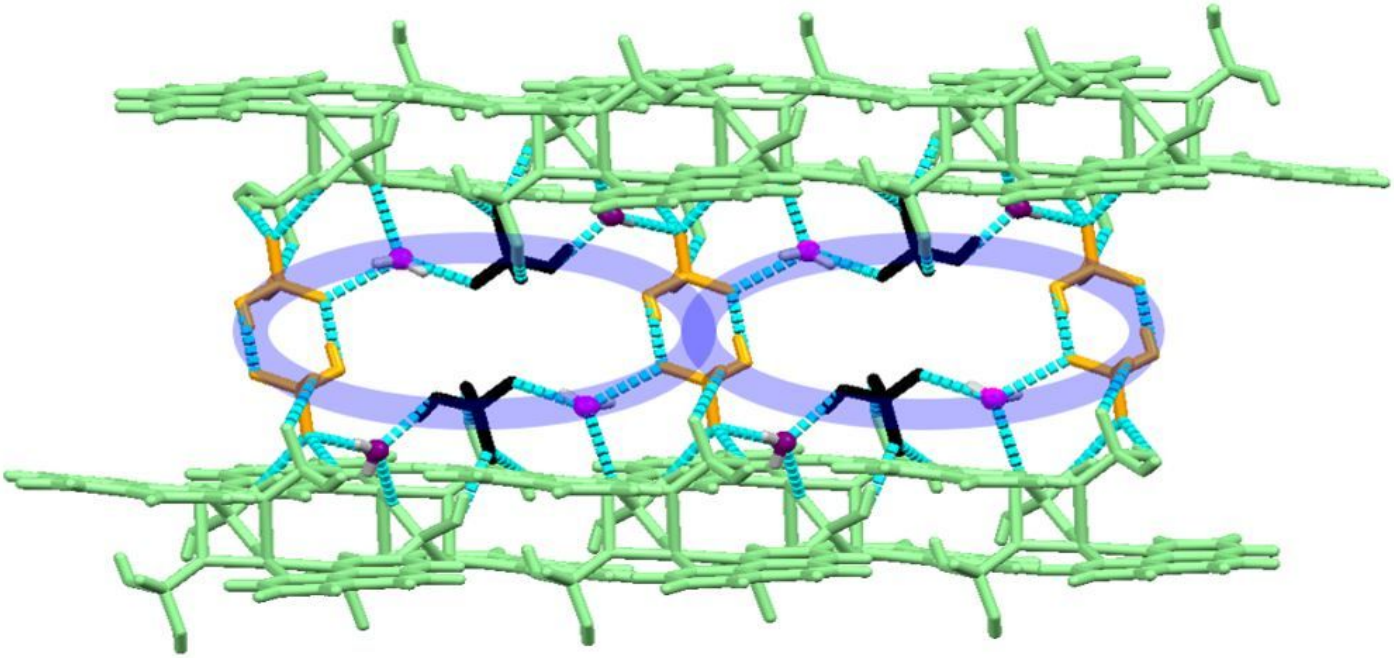

Figure 4

The H-bonds interaction between [(H2PO4)(H2O)]nn- anion large ring, Ow34 (magenta), Ow36 (purple), and [Cu2(phen)2(H2PO4)3] in Cu1, Cu2 binuclear group (light green).

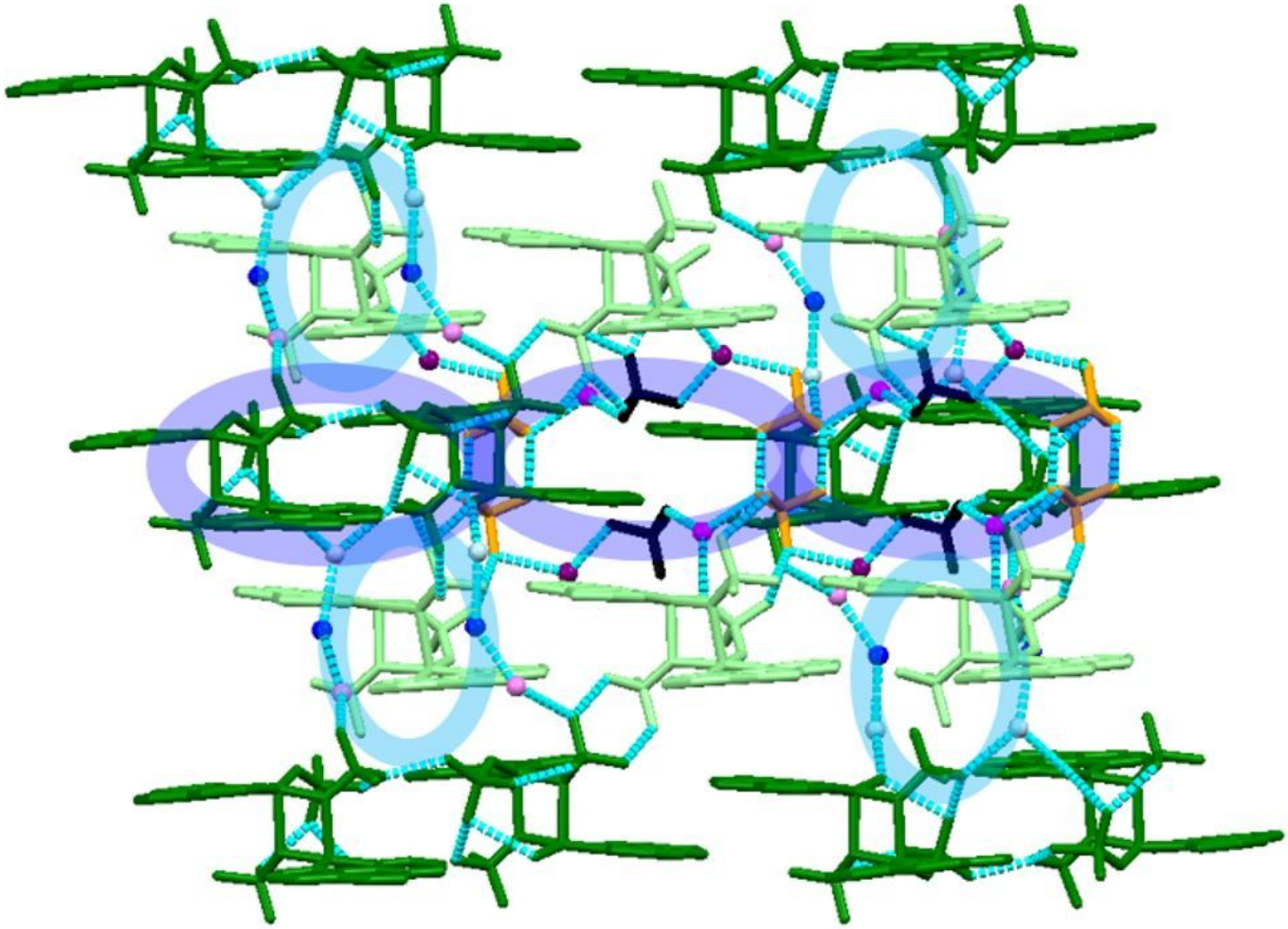

Figure 5

3D H-bonds network structure of complex 1.

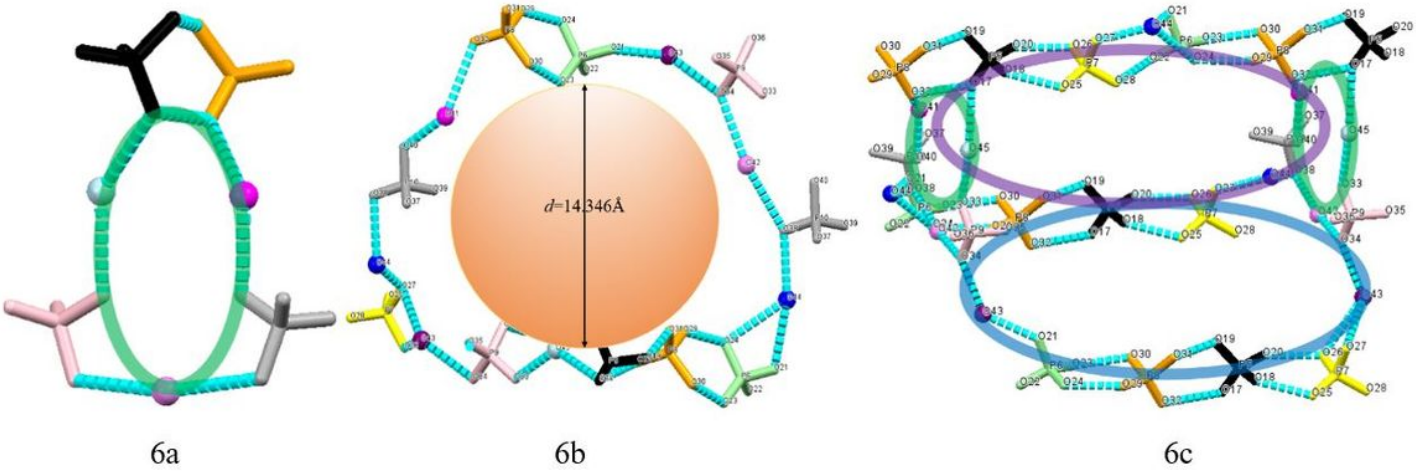

Figure 6

For complex 2: (6a) The eleven rings forming by three H2O with two (HPO4)2- and two (H3PO4). (6b) The twenty-nine ring formed by five H2O with three (HPO4)2- and seven (H3PO4). (6c) The twenty-seven ring formed by three H2O with four (HPO4)2- and seven (H3PO4); The twenty-seven ring formed by three H2O with three (HPO4)2- and eight (H3PO4); and the thirty-four ring formed by two H2O with four (HPO4)2- and six (H3PO4); Hydrogen atoms are omitted for clarity. The black groups represent [HP(5)O4]2-, The dark grey groups represent [HP(10)O4]2- and the light green, yellow, orange and pink groups represent (H3PO4).

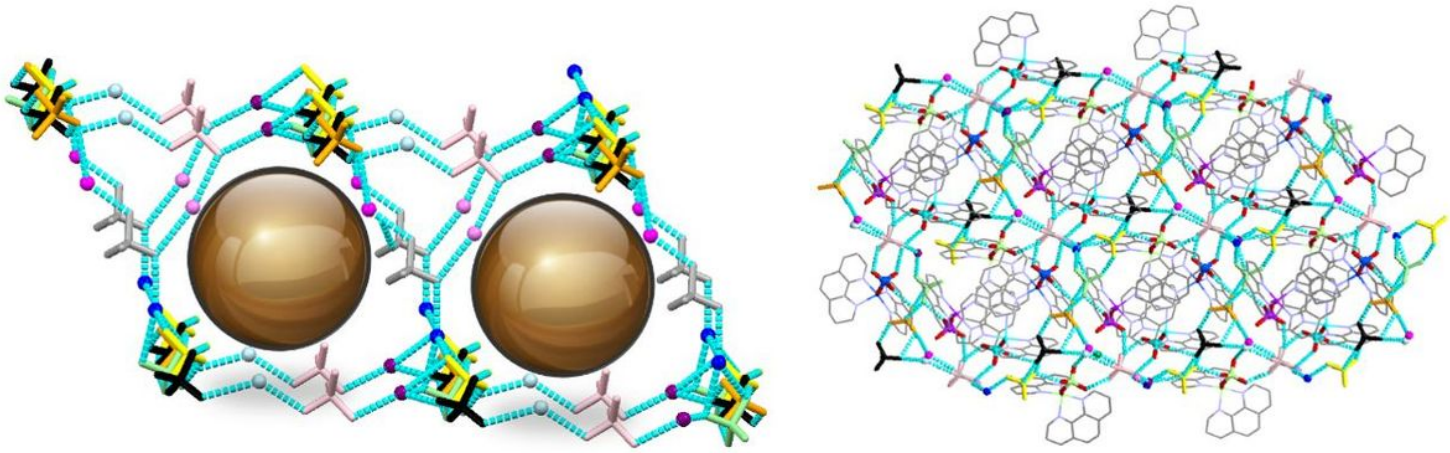

7a 7b

Figure 7

For complex 2: (7a) View of a cage-like structure of guest [(H3PO4)4(HPO4)2(H2O)5]n8n- along the b axis, which contains a sphere of diameter about 14Å. (7b) View of the host [Cu(phen)2(H2PO4)] lying in the cage structure formed by guest supramolecular action.

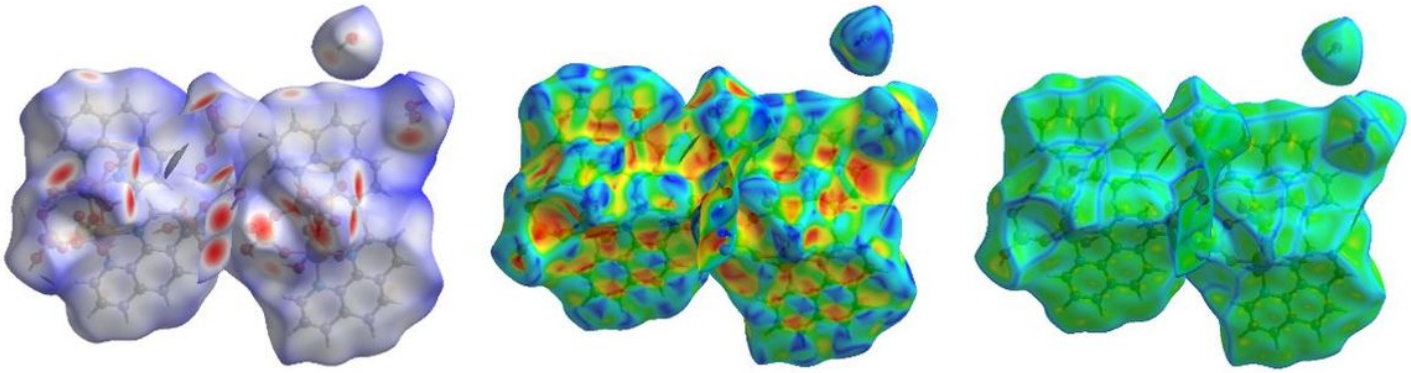

(8a) d_{norm} (8b) shape index (8c) curvedness

Figure 8

Hirshfeld surface mapped with dnorm (a), shape index (b), curvedness (c) for complex 1.

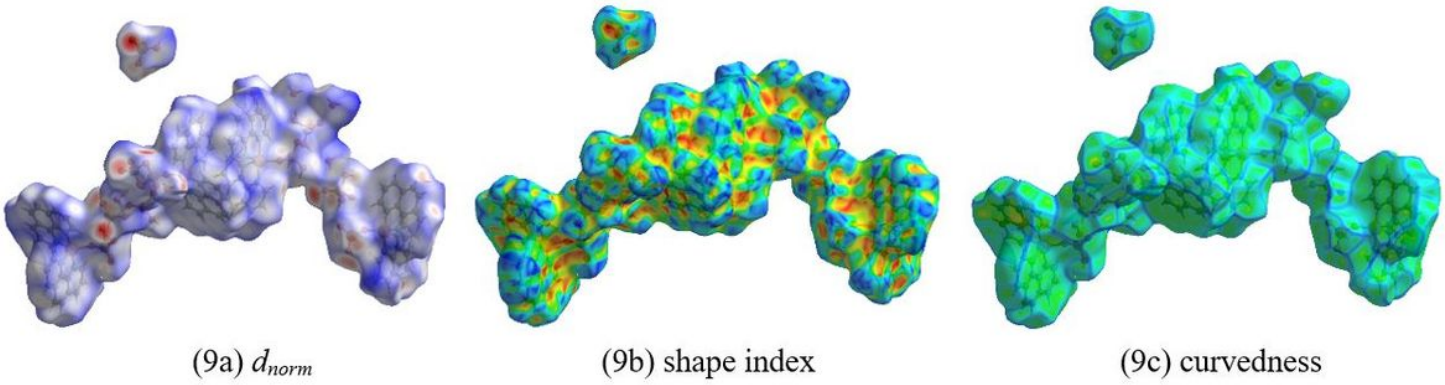

Figure 9

Hirshfeld surface mapped with dnorm (a), shape index (b), curvedness (c) for complex 2.

Figure 10

2D fingerprint plot derived from HS of complex 1.

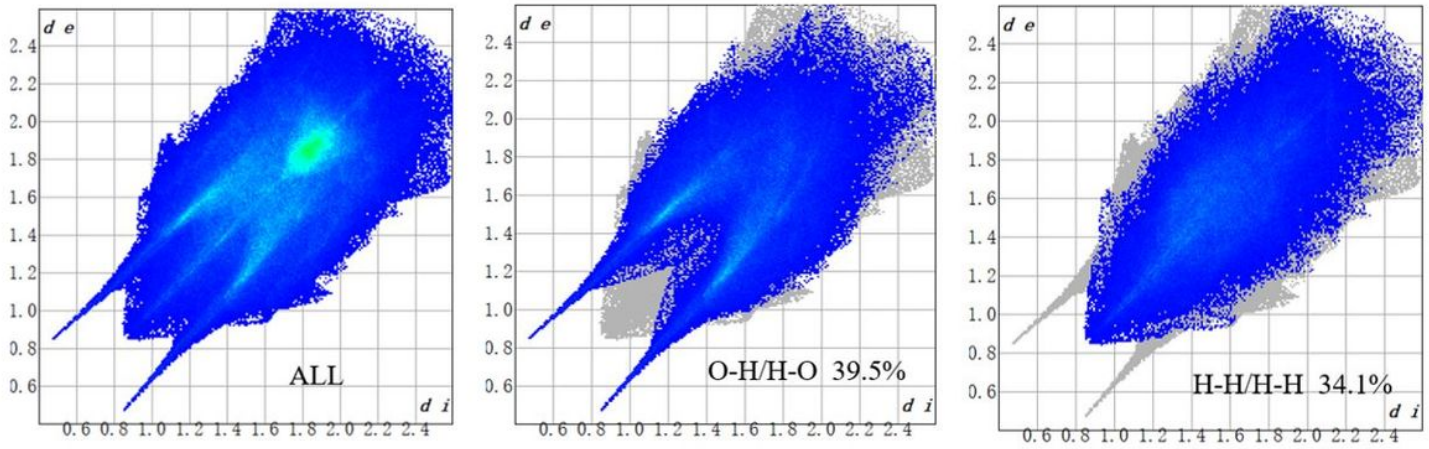

Figure 11

2D fingerprint plot derived from HS of complex 2.

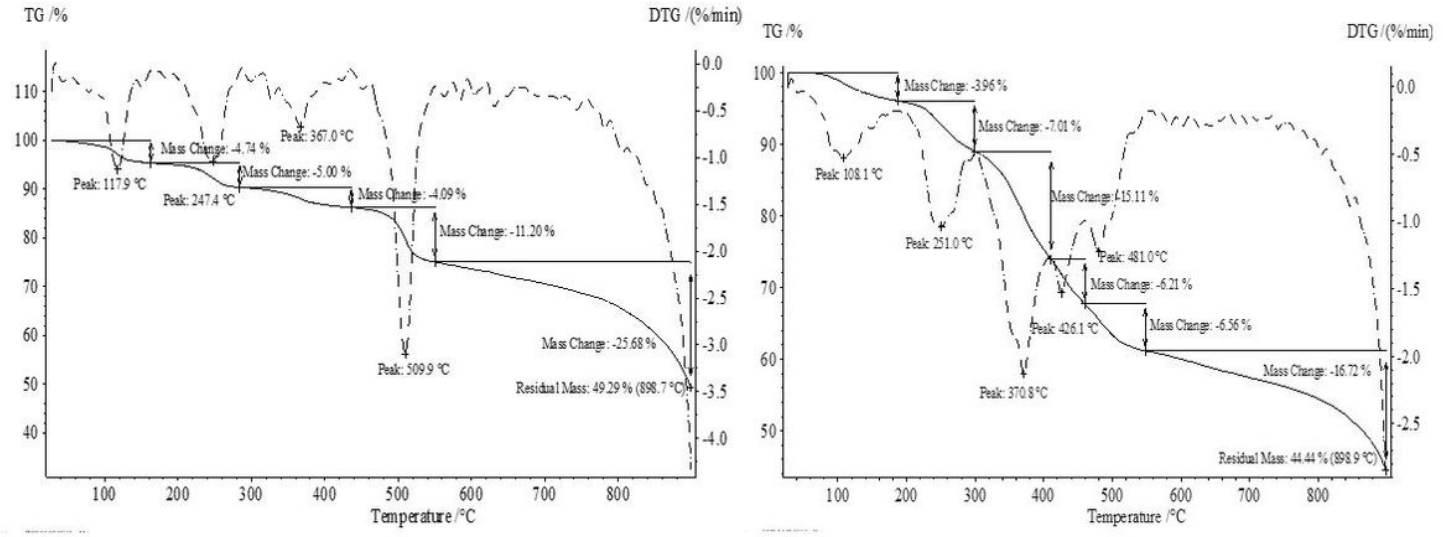

Figure 12

TG and DTG analysis for complex 1 (12a) and complex 2 (12b).

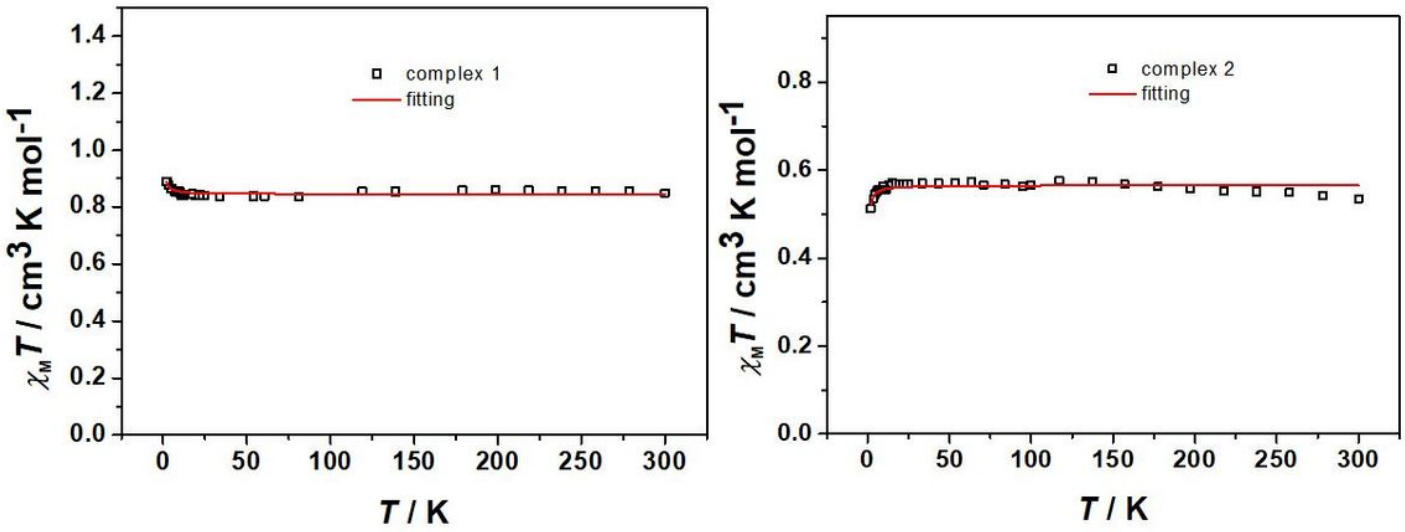

Figure 13

The variable-temperature magnetic properties of complexes 1 and 2. The solid lines represent the best fitting results.

Supplementary Files

This is a list of supplementary files associated with this preprint. Click to download.

- SupportingInformation.doc
- checkcifcomplex1.pdf
- checkcifcomplex2.pdf